Material Studies
Research Highlights

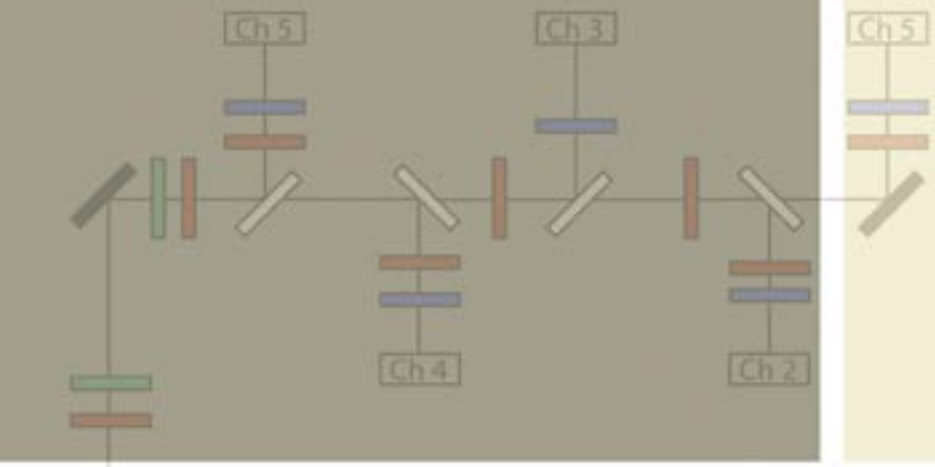

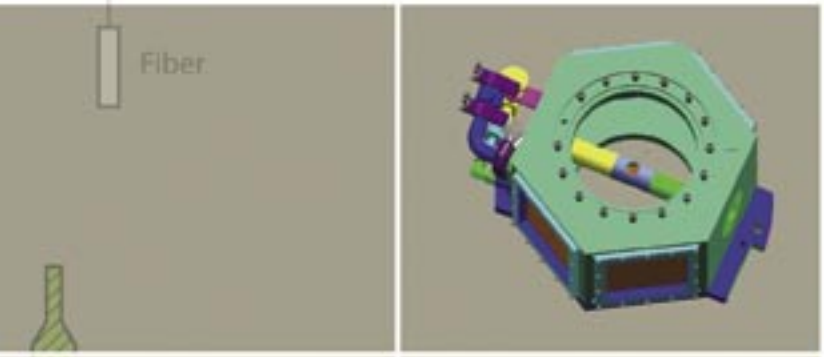

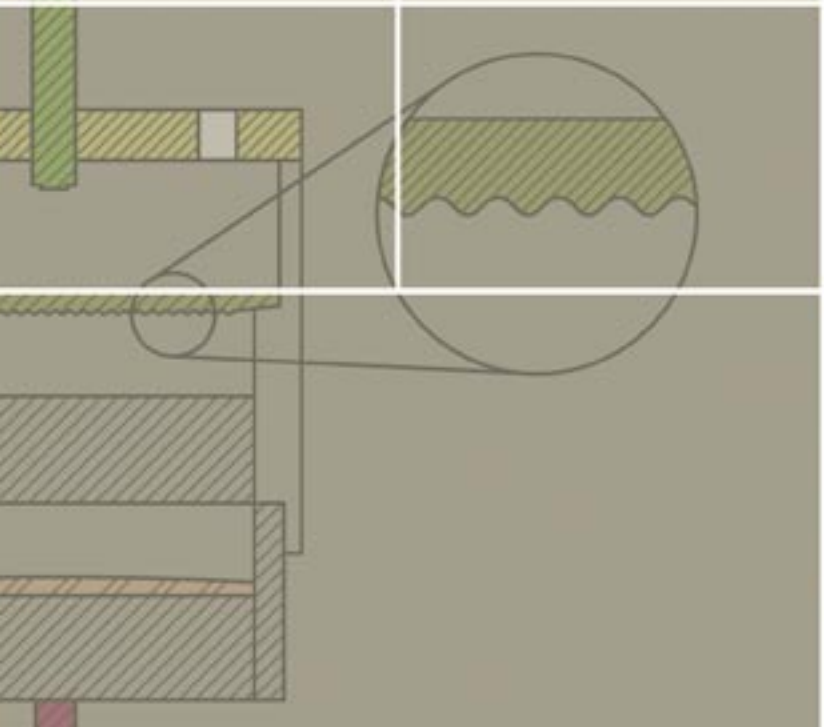

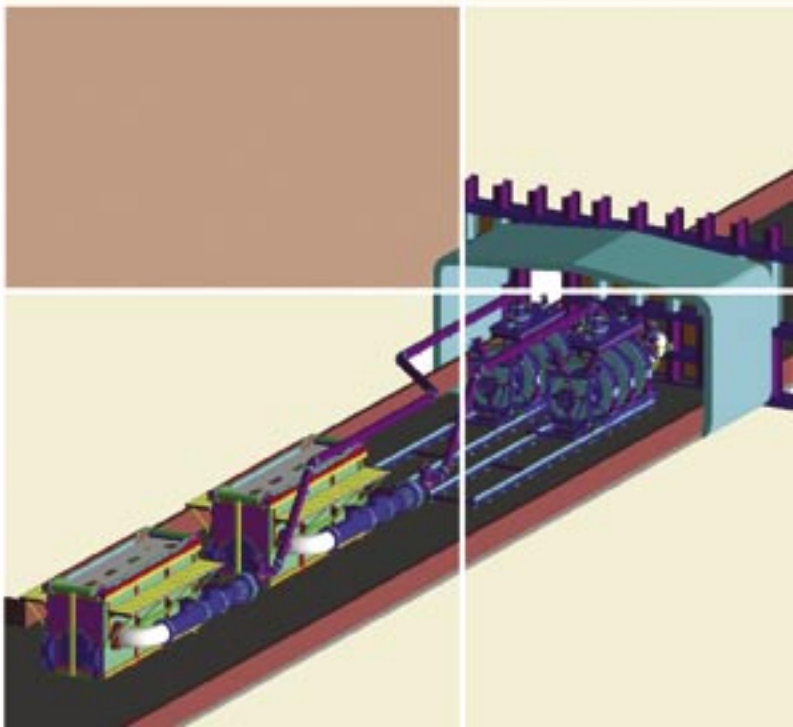

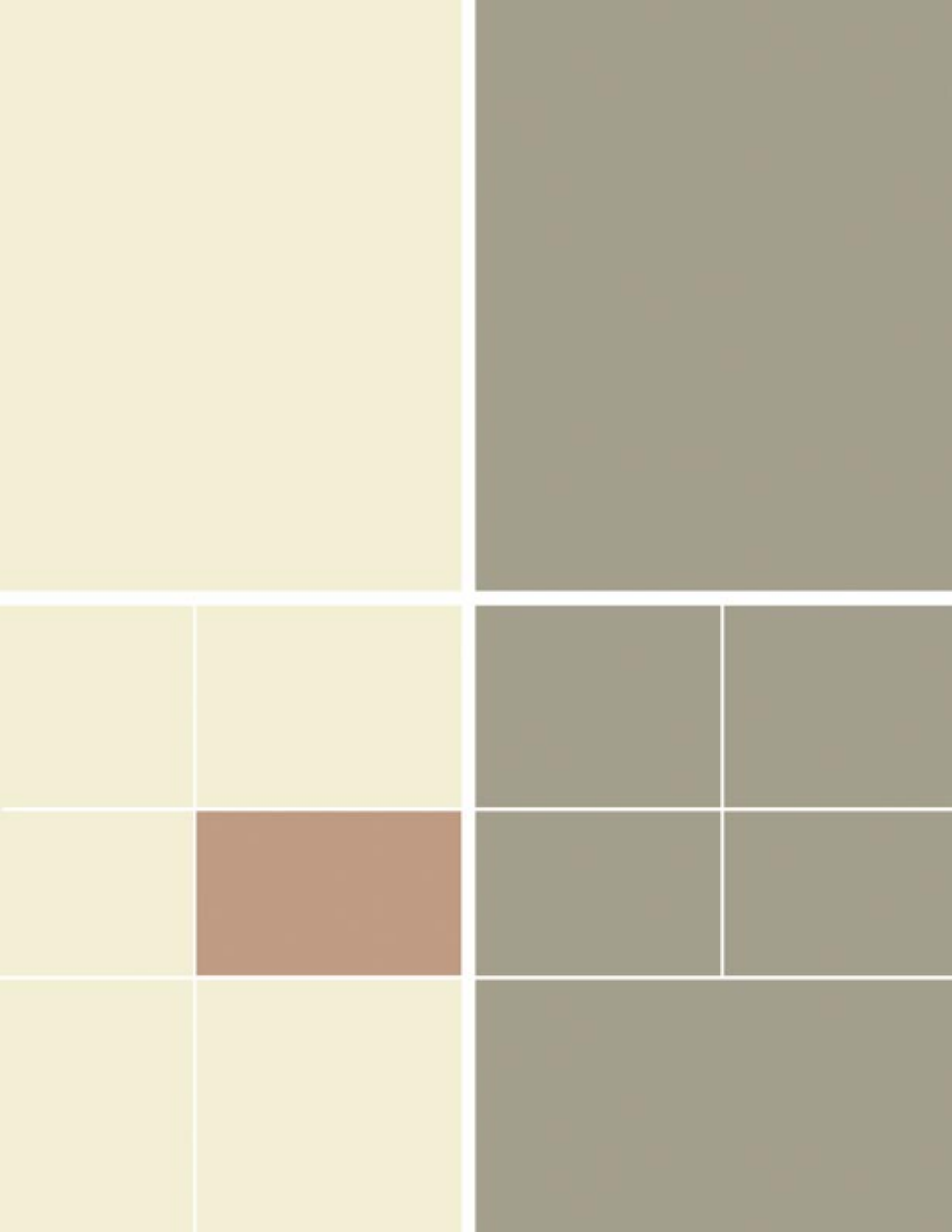

Optical Pyrometry on the Armando Subcritical Experiment

C.M. Frankle, D.B. Holtkamp (P-22), S.D. Borror, R.B. Corrow, J.Crystal, L. Woo (Bechtel Nevada)

The Armando subcritical experiment (SCE) was the final shot in the Stallion series of SCEs, also consisting of two previous shots, Mario and Rocco. The primary objective of the Stallion series was to investigate differences in material properties between cast and wrought plutonium driven by high explosives (HE). The Armando experiment contained two plutonium/HE packages, which were identical except one contained wrought plutonium while the other held cast plutonium. The two packages were also identical to those fired on Mario and Rocco. While Mario and Rocco were primarily diagnosed using point techniques, Armando was primarily diagnosed using an area technique (radiography). However, two diagnostics were common to all three shots—a single-point velocimetry measurement using the velocity interferometer system for any reflector (VISAR) and optical pyrometry.

The optical-pyrometry technique measures the surface temperature of the plutonium as it is heated by the passage of the HE's shock wave. Light is emitted from an ideal blackbody surface based on its temperature in accordance with Planck's law:

$$L_\lambda = \frac{2c^2 h}{\lambda^5 \left(e^{hc/\lambda kT} - 1\right)}. \qquad (1)$$

Here L_λ is the radiance in W/m^2 sr m, c is the speed of light, h is Planck's constant, λ is the light's wavelength, k is Boltzmann's constant, and T is the temperature. In order to perform the measurement, a pyrometer is constructed using high-speed photomultiplier tubes (PMTs) filtered to be responsive to certain wavelength bands. Due to the explosive nature of the experiment, the pyrometer is located remotely from the package. An optical probe collects the light emitted from the plutonium surface and is sent over ~ 100 m of 1 mm diameter optical fiber. High-speed digitizers then capture the signals from the PMTs.

Pyrometry data was successfully returned from Mario, Rocco, and Armando. The data is currently being analyzed.

Pyrometer Design

The pyrometer system was specifically designed to meet the needs of the Stallion SCE series. In other words, the expected range of temperatures and the operating conditions of the overall experiment dictated the selection and layout of components. Armando required two identical pyrometers, one for each plutonium piece. One of our primary considerations was measuring temperatures in the range of ~ 300 °C to ~ 1200 °C, to operate with timing resolution of a few ns, and to coexist with large quantities (many Watts) of 532 nm light from the VISAR lasers. Figure 1 illustrates the experiment's schematics and design. The pyrometer utilizes five channels, three in the visible spectrum and two in the near infrared. Each channel is a 2 in. diam PMT that has a ~ 3 ns rise time. The visible tubes are Hamamatsu R943-02 operating at room temperature, and the near-infrared tubes are Hamamatsu R5509-72 operating at -80 °C. Optical bandpass filters are placed in front of each tube to select a particular wavelength band, which are listed in Table 1.

Referring to Figure 1, the operation of the pyrometer is as follows. First, light from the transporting optical fiber is brought into reasonable focus using a lens. The light then impinges on an OD6 holographic-notch filter which passes all light except those in a 10 nm wide band around 532 nm. The 532 nm light is reflected backward into a beam dump. The notation "OD6" indicates that the intensity of 532 nm light is reduced by a nominal factor of 10^6 in passing through the filter. After passing the first holographic-notch filter, the beam is bent 90° using a turning

Table 1. Wavelength coverage of Armando pyrometers

Channel	Spectral Range (nm)
1	1510–1670
2	1180–1300
3	800–900
4	690–750
5	496–517

RESEARCH HIGHLIGHT
PHYSICS DIVISION

Figure 1. Schematic diagram of the pyrometer.

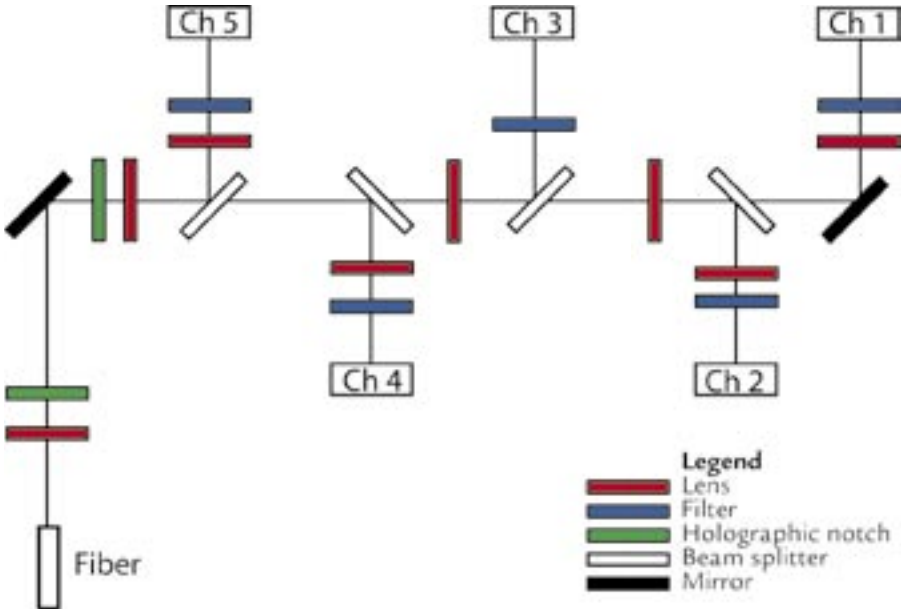

mirror. It then passes through a second OD6 holographic-notch filter for a total reduction of 532 nm light of up to 12 orders of magnitude. The beam then passes through a lens to further adjust the focus before proceeding through a series of dichroic beam splitters. Each beam splitter reflects wavelengths shorter than a cutoff value into the PMT designated to measure a corresponding wavelength band. Each PMT also has a lens in front of it to focus the incident light for optimal geometric coverage of its photocathode. A passband filter is also used with each channel to define the wavelength coverage. The longest wavelengths are sent to channel 1 using a turning mirror instead of a beam splitter.

Armando Experiment Design

The Armando experimental package was designed to allow for simultaneous firing of two plutonium/HE subassemblies, identical except for the initial plutonium shaping technique. These two subassemblies were mounted on the top and bottom of a six-sided (HEX) package (Figure 2). Two radiographic lines of sight, spaced 60° apart, were aligned with four of the six package sides. A tube was mounted through the remaining two sides of the package. At the center of the tube, a double-sided mirror was mounted at a 45° angle to the axis of the tube such that the upper plutonium surface could be viewed through one end of the tube and the lower plutonium surface could be viewed through the opposite end of the tube (Figure 3). The tube had to be made small, so that the two radiographic images could be obtained before the plutonium surface impacted the tube.

The central tube provided optical access for the pyrometry and VISAR diagnostics. Our colleagues at Bechtel Nevada (BN) did an outstanding job at designing an integrated optical probe, incorporating the needs of both the pyrometry and VISAR teams. The VISAR transmit fiber was mounted in a small hole drilled through the center of the two lenses which were mounted at the front of the probe. Return light for the VISAR was then focused on a receive fiber mounted behind the transmit fiber. The larger, 1 mm diameter, pyrometry fiber was mounted off-axis to the probe so that it received light from a spot on the plutonium surface approximately 1 cm away from the spot illuminated by the VISAR laser. This scheme is illustrated in Figure 4. A photograph of a completed probe is shown in Figure 5. One probe was inserted in each side of the hex package central tube.

Figure 3. The Armando HEX package showing the location of the mirror in the center of the combined pyrometer/VISAR probe tube.

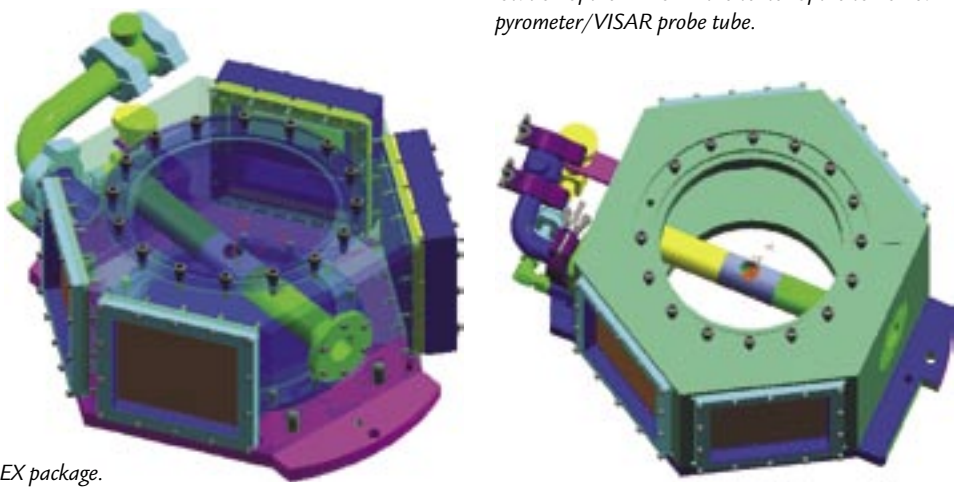

Figure 2. The Armando HEX package.

Figure 4. Schematic diagram of the combined pyrometry/VISAR probe.

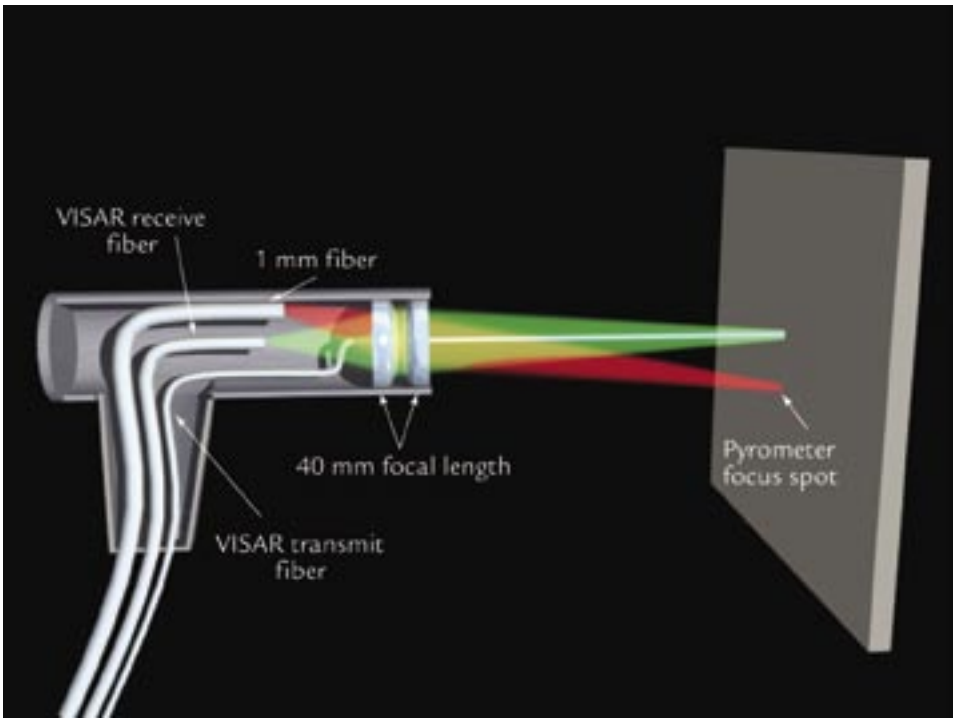

Pyrometer Operation

Before the experiment, each pyrometer must first be calibrated with a blackbody source to obtain the relationship between measured output voltage on the PMTs and the incident radiance. The procedure is to set the blackbody at a specified temperature and measure the output voltage on each PMT. The radiance for each channel can then be calculated by

$$L_i(\lambda,T) = \int_{\Delta\lambda_i} \varepsilon_i L_\lambda d\lambda, \qquad (2)$$

where L_λ is as before and ε_i is the emissivity. For a blackbody, the emissivity is unity and the radiance is easily calculated using the known bandpass characteristics of each filter. An example of the resulting calibration data is shown in Figure 6. Note that the PMTs are linear from a few mV to a few tens of volts. We performed these calibrations using the complete optical system, including pyrometer, fiber, optical head, and hex package tube and mirror.

In the experiment, we measure a voltage, which has a corresponding radiance $L_i(\lambda,T)$, for each pyrometer channel. However, unlike in the calibration case, we do not know the emissivity of the plutonium surface. Hence, we have N measurements but N+1 unknowns, corresponding to the N unknown dynamic emissivities plus the temperature. In order to address this difficulty, we make two assumptions:

(1) the radiances all correspond to a single temperature, even though the dynamic emissivities may be different (emissivity is in general wavelength dependent) and

(2) that the dynamic emissivity can be bound using known properties of the material.

For example, the emissivity must have an upper bound of 1, corresponding to that of a blackbody. A reasonable lower bound might be the static emissivity of a freshly machined or polished surface. With these assumptions an additional 2N of constraints are introduced, allowing a temperature (and associated uncertainty) to be derived. Note that due to the shape of

Figure 5. Photograph of completed pyrometry/VISAR probe.

Figure 6. Example calibration data.

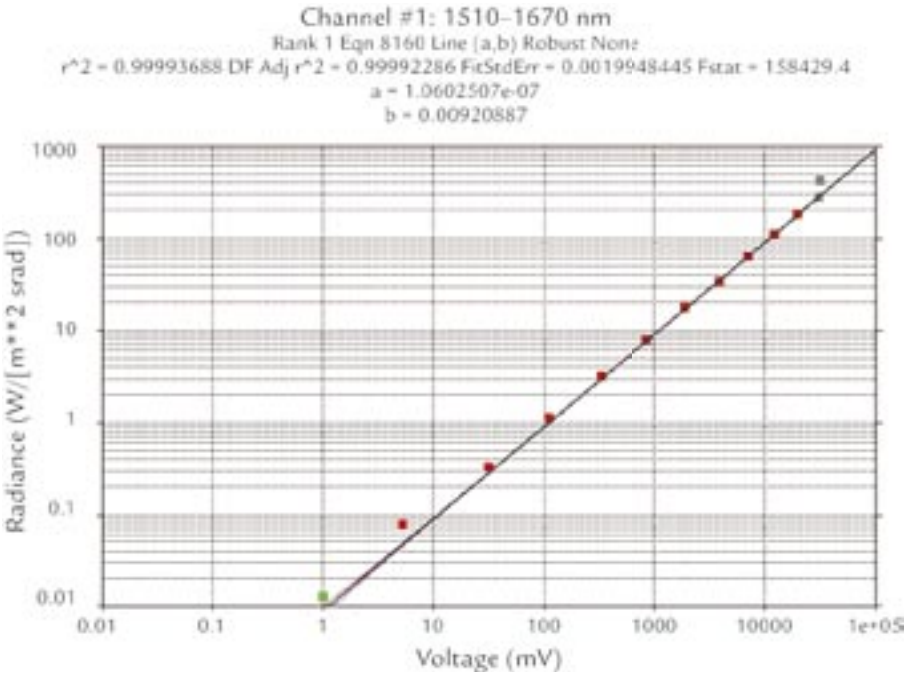

the radiance curve, the shorter wavelength channels most strongly constrain the temperature.

Armando was successfully fired on May 25, 2004. Pyrometry data was returned on all channels, and the analysis of the data is ongoing. However, our preliminary analysis clearly shows measurable differences in the radiance from the cast and wrought parts—in a manner similar to that observed between Mario and Rocco.

Acknowledgment

We gratefully acknowledge the contributions of the many individuals at LANL and BN who helped make this experiment possible. This work was funded by the U.S. DOE Office of Defense Programs.

For further information, contact Chris Frankle, 505-665-4138, cfrankle@lanl.gov.

Armando: The Final Subcritical Experiment in the Stallion Series

R.D. Fulton

Armando was the final subcritical experiment (SCE) in the Stallion series. The Stallion series of experiments (Vito/Etna, Mario, Rocco, and Armando) were designed to evaluate high-explosive (HE) driven properties of cast and wrought plutonium; the cast and wrought materials being representative of the materials produced via the different manufacturing processes employed at Rocky Flats and LANL. Specific properties investigated were ejecta production, spall features, and surface temperatures. Ejecta is defined as the small particulate matter "ejected" from the surface of a solid when a strong shock wave interacts with the surface. Spall is a general term for bulk material failure near the surface of a solid created by a strong shock interacting with the surface. Both of these phenomena depend upon the material properties: material strength, grain size, impurities, etc., as well as the strength and temporal profile of the shock pressure. The surface temperature is an important constraint upon the final state of the shock-driven metal that will be important in a full understanding of the behavior of the material.

Vito/Etna was a joint experiment conducted with the Aldermaston Weapons Establishment (AWE) located in the United Kingdom that concentrated on ejecta. Rocco and Mario were separate cast and wrought experiments that examined the phenomena of interest with a suite of point diagnostics. These diagnostics provided either specific time arrival information at a single spatial point or a continuous time record of some material property at a single spatial point. Armando was designed to complement and extend the measurements of Rocco and Mario by combining the two experiments into a single package and radiographing the behavior at two separate times along equivalent lines of sight. The paraphrased paradigm is: a picture is worth a thousand pins.

Diagnostics and Package Composition

HE diagnostics equivalent to those used on Rocco and Mario were implemented to verify identical HE performance. These consisted of a series of shorting switches combined with a microwave interferometer strip laid out symmetrically on the HE package to measure detonation times and velocities. Point VISARs (Velocity Interferometer System for Any Reflector) and optical pyrometers (that provide a measure of the surface temperature) were also implemented to verify equivalent behavior of the surface properties. The primary diagnostic for Armando was x-ray radiography along two equivalent axes separated by 60°. Physics packages identical to the Rocco and Mario packages were combined in a HEX package (6-sides or High-Energy X-ray) vertically separated with the free surfaces facing one another. This geometry allows for exactly equivalent radiographs to be taken of the two materials at the same time in their evolution. The third axis of the HEX package is used for VISAR/pyrometry access.

The experimental package is contained within a 3 ft diam (inside diameter) containment vessel. This vessel and the camera box that houses the scintillator and camera system are placed within a "zero room" created by a large bulkhead completely sealing off the end of the U1a.05 drift. Thin radiographic windows in the bulkhead and vessel allow the x-rays to pass through the package and the containment vessel with minimal attenuation. Originally designed so as to expend the zero room, fielding the experiment within a containment vessel allows for the reuse of the zero room for multiple experiments and provides multiple redundant containment (Figure 1).

The Cygnus sources extend down the drift externally to the zero room. They are composed of a Marx bank system contained in large oil-filled tanks that pulse-charge adjacent pulse-forming lines (PFL). The output of the PFL is a short pulse (~ 60 ns), large-amplitude (~ 1 MV) electrical pulse that propagates down an 8 in. diam, water-filled, coaxial transmission line. This electrical pulse is coupled into the inductive voltage adder (IVA) cells that add the voltage

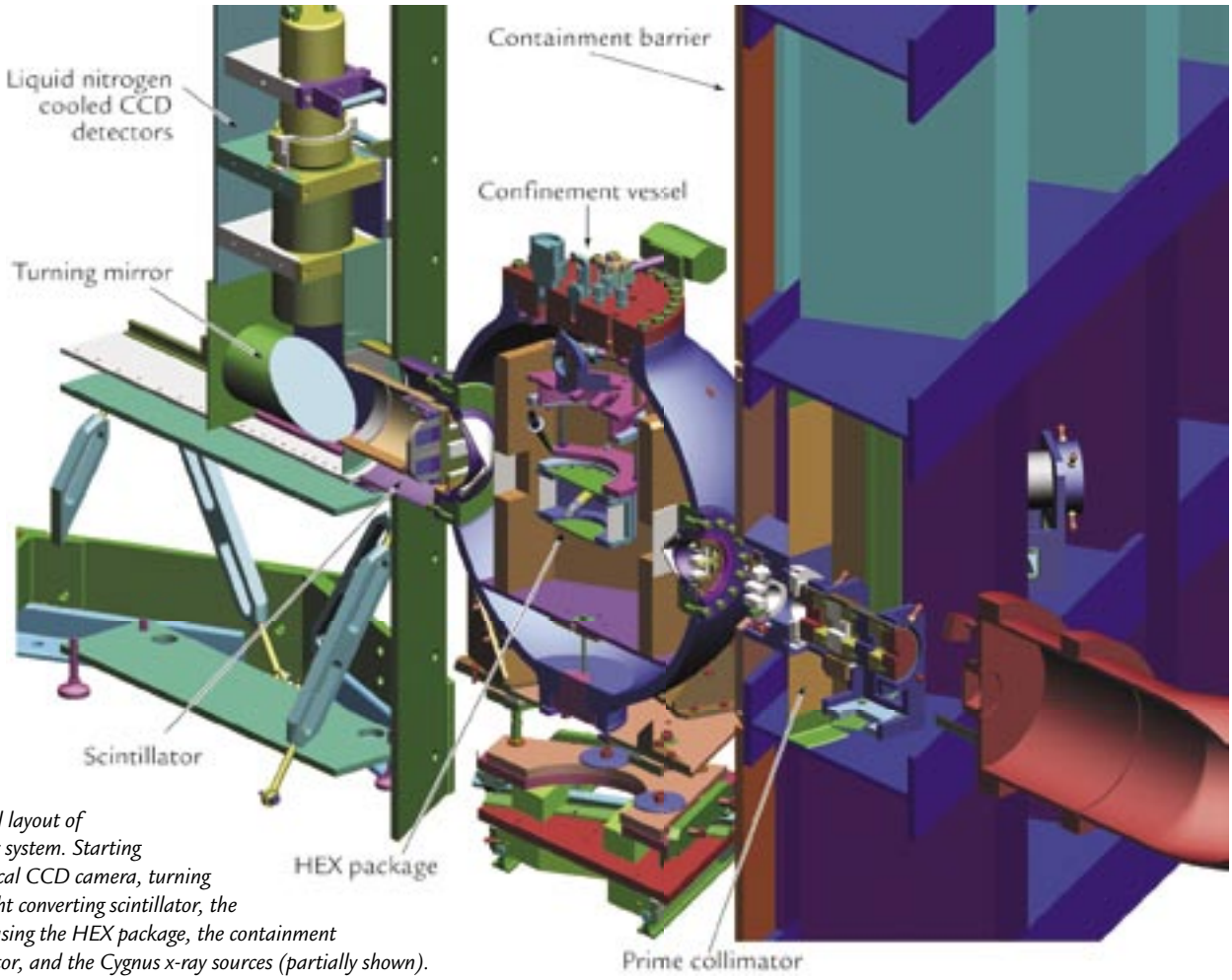

Figure 1. Experimental layout of Armando radiographic system. Starting from the left: the vertical CCD camera, turning mirror, the x-ray to light converting scintillator, the confinement vessel housing the HEX package, the containment barrier, prime collimator, and the Cygnus x-ray sources (partially shown).

in parallel to produce a 2.25 MV, low-impedance drive pulse for the rod-pinch diode. This last stage of voltage addition is accomplished in a high-vacuum suitable for diode operation. The expertise of Sandia National Laboratories (SNL) and Titan/Pulse Sciences Division (PSD) were instrumental in applying the technology developed at SNL to realize a robust and flexible pulse-powered driver capable of operating reliably underground.

Radiography and Detector Systems

The radiography employed on Armando represents a significant advance in the performance of medium-energy radiography. It has been the result of a multiyear, multi-Laboratory effort involving LANL, SNL, Bechtel Nevada (BN), the Naval Research Laboratory (NRL), AWE, Titan/PSD, and Mission Research Corporation (MRC). Many innovations have been combined to lead to this advance in performance, but perhaps the most important has been the effective realization of the rod-pinch diode originally developed at NRL. The rod pinch has a similar geometry to standard x-ray diodes in use in industrial flash x-ray sources for several decades. However, researchers at NRL realized that when operated at low impedance (Z), the diode would transition from classic space charge limited (SCL) flow into magnetically limited (ML) flow whereby the electrons would be transported to the end of the central anode rod and then "pinch" producing a very bright, small diameter x-ray source (Figure 4). The Cygnus x-ray source was designed to provide a low-impedance (high-current) source of voltage to effectively drive the diode into the ML regime. Measurements have demonstrated a 1 mm diam x-ray spot size producing 4 rad at 1 m in a reproducible manner.

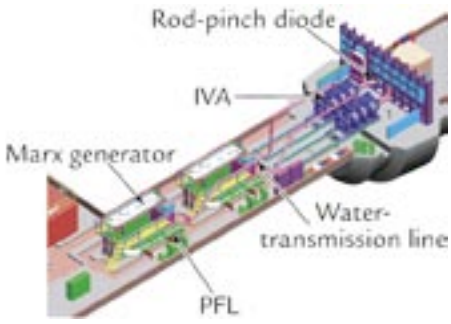

Figure 2. Layout of Cygnus x-ray sources in U1a.05 drift. Confinement vessel and camera box are not shown in this view.

The detector system is equally innovative. It combines technologies developed for Dual-Axis Radiographic Hydrodynamic Test (DARHT) and proton radiography to create a very high-resolution imaging system. It functions by converting the x-rays transmitted through the experimental package into visible light in a tiled LSO (lutetium oxyorthosilicate) scintillator. The light produced is transported by a low-f/# lens system to a LN_2-cooled charged-coupled-device (CCD) chip that captures and records the image. In order to preserve maximum image resolution, the combined CCD camera system is not gated; all time resolution therefore derives from the flash nature of the illuminating x-ray pulse. While providing optimum resolution, this technique introduces a risk to the experiment, in that the scintillator-camera combination must be maintained in a light tight configuration throughout the HE detonation and long enough thereafter (~ 90 s) for the information to be read out of the CCD camera system to a remote data logging computer.

Results

The results of Armando have provided valuable data for stockpile stewardship. The HE diagnostics demonstrated identical performance of the HE detonation in all four packages: Rocco, Mario, and Armando cast and wrought. The VISAR measurement demonstrated that the measured surface velocity was reproduced within error bars. The radiography provided detailed subsurface data on the spalled material with a resolution and precision previously unobtainable. Radiographic data was obtained at two times allowing comparison with the VISAR data. The inferred velocity was in excellent agreement, further enhancing confidence in the accuracy of the results.

Figure 3. A view of the U1a.05 drift. The "zero room" bulkhead is seen with the two IVA structures fed by the water-filled coaxial transmission lines in the foreground.

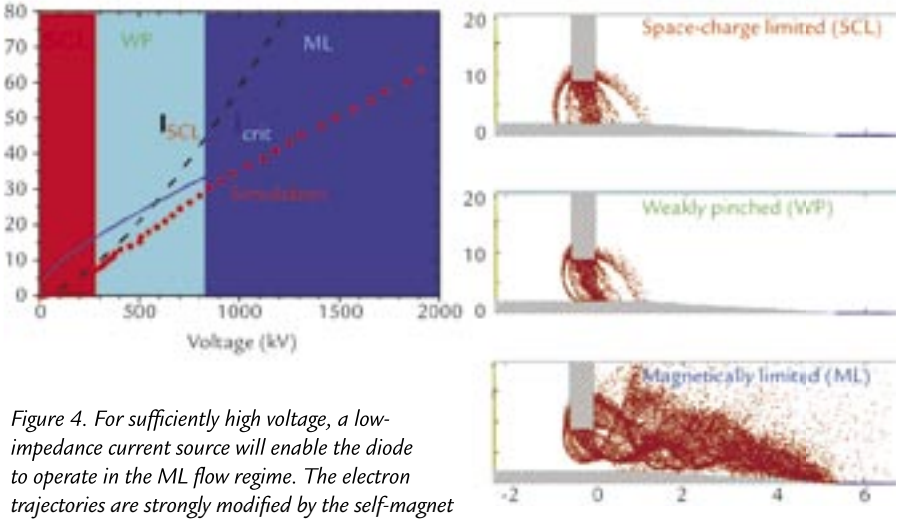

Figure 4. For sufficiently high voltage, a low-impedance current source will enable the diode to operate in the ML flow regime. The electron trajectories are strongly modified by the self-magnet field and propagate to the end of the anode producing an intense, small spot of x-rays. Dimensions are in millimeters. Figure courtesy of NRL.

Acknowledgment

A great many people in many divisions (Physics, Dynamic Experimentation, Engineering Sciences and Applications, Material Science and Technology, Applied Physics, Nuclear Materials Technology, Health, Safety, and Radiation Protection, and Earth and Environmental Sciences) at LANL worked in a very productive partnership with SNL, Titan PSD, NRL, MRC, and BN to develop the technology and execute the Armando SCE. It is not possible to call out every individual in this format, but their efforts and dedication to this project are deeply appreciated.

For further information, contact Doug Fulton, 505-667-5005, fulton_robert_d@lanl.gov.

Material Strength under Shock and Shock-Free Loading Conditions

D.L. Preston, R.T. Olson (P-22), A. Kaul, R.J. Faehl (X-1)

Numerical simulations of explosively driven deformation and high-velocity impacts require rate-dependent models of material strength. The main challenge in constructing such models is the wide range of thermodynamic and mechanical conditions that occur in particular solid-flow processes: plastic strains to several hundred percent, plastic strain-rates up to 10^{11} s^{-1}, pressure to several megabars, and temperatures up to melt. Ideally, a material-strength model would be based on internal-state variables that provide a complete representation of the microstructural state and its evolution, but our limited knowledge of dislocation, grain-boundary dynamics, and phase-transformation kinetics currently precludes the construction of such a model. Nevertheless, steps towards developing such a material-strength model have been taken by Follansbee and Kocks who used the mechanical threshold stress (MTS, plastic-flow stress at 0 K) as a structure parameter.[1] Their MTS model only accounts for thermally activated dislocation motion, thus it cannot be reliably applied at strain rates much above 10^{4} s^{-1}. This limitation was overcome by Preston, Tonks, and Wallace (PTW) who developed a model of material strength[2] applicable at strain rates from 10^{-3} s^{-1} to 10^{12} s^{-1}. The PTW model has been implemented in several hydrodynamic codes at LANL and has been successfully used to simulate Taylor cylinder impacts, explosively driven systems, and high-velocity impact cratering.[3] It should be mentioned that the 25-year-old rate-independent Steinberg-Guinan (SG) material-strength model is also still used in certain numerical simulations at LANL.[4]

Adiabatic Shear-Band Formation and Time-Dependent Material Strength

The PTW, MTS, and SG models are all founded on the assumption that the plastic flow is spatially homogeneous, that is, the plastic deformation is not localized. However, recent experiments on copper by V.A. Raevsky *et al.* at the All-Russian Research Institute of Experimental Physics (VNIIEF) show that this assumption can break down under both shock and shock-free loading conditions.[5] (These experiments were funded by LANL under the Gordon/Ryabev agreement.) The shock experiments are at strain rates above 10^{9} s^{-1}, while the shock-free experiments are used to reduce strain rates to $10^{5–7}$ s^{-1}. The Raevsky experiments, which are described in more detail below, involve loading copper plates with surface perturbations by explosive detonation and then measuring the perturbation amplitude as a function of time. In recent experiments at VNIIEF, some of the plates were recovered for subsequent metallographic analysis. Remarkably, shear bands, localized regions of large plastic deformation, were present in the recovered samples loaded to pressures above 27 GPa. The shear-band density increases in the direction of the compression wave's propagation into the sample, probably as a result of the increase in the strain rate as the compression wave steepens into a shock wave. Raevsky *et al.* have also carried out experiments in collaboration with Lawrence Livermore National Laboratory (LLNL) that show shear-band formation in 6061-T6 aluminum.[6]

We can deduce the implications of these findings for material strength by considering the formation and structure of a shear band. Approximately 90% of the work done during plastic deformation is converted into heat. If the strain rate in a region is sufficiently high, as is the case in a high-pressure shock front, then very little heat diffuses out of the region during its deformation, thus the heating is nearly adiabatic. If the decrease in strength due to the increase in temperature exceeds the increase in strength from work hardening, then the plastic deformation becomes unstable, resulting in the formation of an adiabatic shear band. The total plastic

strain in the shear band can be quite large: 500%–800%. The corresponding temperature rise is of order 10^3 K. The time scale for heat flow away from the hot shear band is $\tau_Q = w^2/\kappa$, where w is the width of the shear band and κ is the thermal diffusivity. As an example, for $w = 10\ \mu m$ and $\kappa = 0.1\ cm^2\ s^{-1}$ (characteristic of steels) we find $\tau_Q = 10\ \mu s$. The macroscopic (spatially averaged) strength (flow stress) will change during the time, τ_Q, required for temperature equilibration around the shear bands. Therefore, the heterogeneity causes the macroscopic material strength to be time dependent.

In view of these considerations, it is no surprise that none of our strength models agree with the Raevsky data on copper (Figure 1). The observed rate of perturbation growth is much greater than the predicted growth rate, which implies that the actual strength is less than that predicted by the models. This is consistent with the presence of hot shear bands in the copper. Unknowns in the Raevsky experiments such as the absolute pressure determination, experiment-to-experiment variability, and the unrealistically small error bars as determined from x-radiographs, raise questions about the overall accuracy of the Raevsky data. Even so, refinements in the Raevsky technique are not expected to bring the data into agreement with calculations based on current strength models.

Future Experiments Based on the Raevsky Technique

Efforts are currently underway in Physics (P) and Applied Physics Divisions to incorporate the effects of shear bands in the PTW model. Experimental data to validate the generalized model are absolutely essential. P Division is currently planning experiments that leverage upon the technique and data of Raevsky in order to create a validation database. These experiments will provide validation data precisely where the PTW model and other rate-dependent models (e.g., MTS and the LLNL Steinberg-Lund model) are least reliable, that is, at strain rates between $10^5\ s^{-1}$ and $10^8\ s^{-1}$ and strains up to several hundred percent, which are the conditions commonly achieved under explosive loading or high-velocity impact of metals. Furthermore, the development of this experimental capability will allow us to investigate materials not studied by Raevsky. The first experiments will be done in collaboration with Raevsky at VNIIEF and then a large suite of additional experiments will be conducted at LANL.

The Raevsky technique utilizes a flat metal plate with perturbations of known wavelength and amplitude machined into the surface. High explosive (HE) is used to generate either shock or shock-free planar loading of the plate. The amplitude of the Rayleigh-Taylor unstable perturbations is measured from x-radiographs acquired as a function of time (Figure 2). This technique can be used to generate pressures in the metal sample in excess of 80 GPa with strain rates ranging from 10^4 to $10^{10}\ s^{-1}$.

The preliminary experiments to be performed at VNIIEF will use diagnostics and well-characterized copper samples from LANL. These experiments will duplicate exactly those previously performed by Raevsky and, as a result, will allow for a direct comparison to the reported Raevsky data. This comparison is essential, for if LANL is to utilize the Raevsky data for model validation purposes, we must corroborate the results and analyze their uncertainties. We currently lack information about repeatability of sample preparation, drive conditions, and absolute peak pressure. It is for this reason that LANL will supply the samples and field a high-precision velocity-measurement diagnostic. Further, the reported accuracy of perturbation amplitudes as determined from radiographic analysis seems to be unrealistically high based upon the resolution limitations present in the VNIIEF x-ray system. The LANL x-ray system to be fielded will provide multiple radiographs per experiment with a small improvement in amplitude resolution. Successful completion of these joint experiments will allow us to define a level of confidence in the reported Raevsky

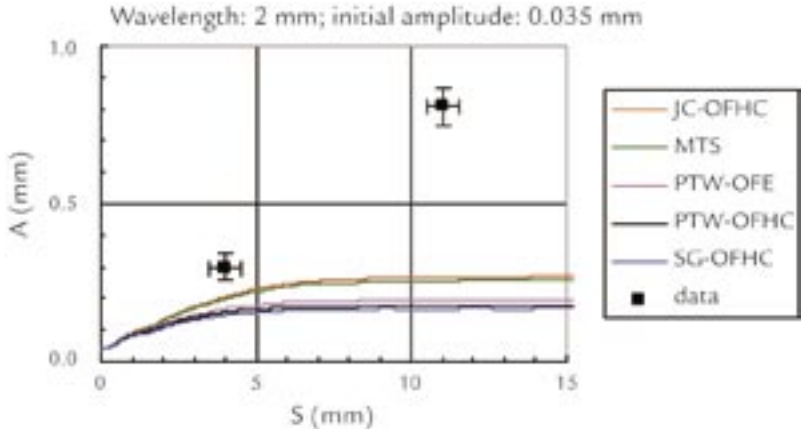

Figure 1. Perturbation amplitude versus the distance traveled by the copper plate due to shock-free loading to a peak pressure of 40 GPa: comparison of numerical simulations using the MTS, PTW, SG, and Johnson-Cook (JC) strength models to Raevsky's data.

data. The shock-free copper experiments will be continued at LANL to obtain a complete validation data set throughout the range of conditions where no other reliable data are available. The HE arrangement and quantity will be altered to control the strain rate and peak pressure through the range 10^5–10^8 s^{-1} and 20–70 GPa, respectively. Sample strain (up to ~ 250%) will be controlled through the wavelength and amplitude of the perturbations. Repeatability of the drive conditions and sample preparation will be ensured with sample velocimetry and material characterization. Amplitude growth will be measured via multiple repetition, low-energy flash x-radiography and will provide the measurable quantity to compare with hydrodynamic computations.

The results of hydrodynamic code simulations using the generalized PTW model will be compared to the extensive validation data set obtained at LANL and VNIIEF. Progressively more realistic representations of shear bands will be incorporated in the generalized model until good agreement with the data is achieved. We should emphasize that the Raevsky technique is currently the only means of obtaining accurate validation strength data at plastic strain-rates exceeding 10^5 s^{-1}, rates that are typical of explosively driven systems and high-velocity impacts.

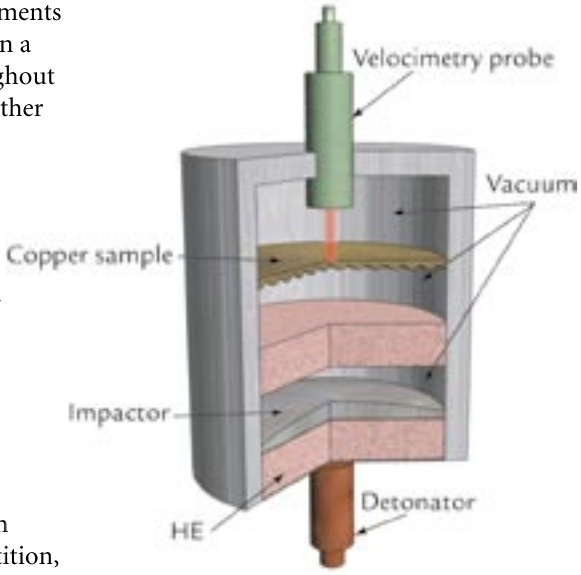

Figure 2. A schematic illustrating the Raevsky design for shock-free instability growth experiments. The radiographic line-of-sight is perpendicular to the plane of the paper.

References

1. P.S. Follansbee and U.F. Kocks, "A constitutive description of the deformation of copper based on the use of the mechanical threshold stress as an internal state variable," *Acta Metallurgica* **36**, 82–93 (1988).
2. D.L. Preston, D.L. Tonks, and D.C. Wallace, "Model of plastic deformation for extreme loading conditions," *Journal of Applied Physics* **39**, 211–220 (2003).
3. R.F. Davidson and M.L. Walsh, "Constitutive modeling for hypervelocity cratering," *AIP Conference Proceedings* **370**, 1159–1162 (1996).
4. D.J. Steinberg, S.G. Cochran, and M.W. Guinan, "Constitutive model for metals applicable at high-strain rate," *Journal of Applied Physics* **51**, 1498–1504 (1980).
5. V.A. Raevsky, All-Russian Institute of Experimental Physics (VNIIEF), Report to LANL on Task 3.1 under Agreement 37713-000-02-35, (2003).
6. V.A. Raevsky, All-Russian Institute of Experimental Physics (VNIIEF), Final Report to LLNL under Agreement B512964, (2002).

Acknowledgment

We would like to thank Dr. Victor A. Raevsky and his collaborators at the VNIIEF for several very informative discussions of their perturbation growth experiments.

For further information, contact Dean Preston, 505-667-8968, dean@lanl.gov.